Biochimica et Biophysica Acta 1787 (2009) 60–67

Contents lists available at ScienceDirect

Biochimica et Biophysica Acta

journal homepage: www.elsevier.com/locate/bbabio

Megacomplex organization of the oxidative phosphorylation system by structural analysis of respiratory supercomplexes from potato

Jelle B. Bultema [a], Hans-Peter Braun [b], Egbert J. Boekema [a,*], Roman Kouřil [a,*]

[a] Department of Biophysical Chemistry, GBB, University of Groningen, Nijenborgh 4, 9747 AG Groningen, The Netherlands
[b] Institute for Plant Genetics, Faculty of Natural Sciences, Universität Hannover, Herren-häuser Str. 2, 30419 Hannover, Germany

ARTICLE INFO

Article history:
Received 2 September 2008
Received in revised form 27 October 2008
Accepted 31 October 2008
Available online 13 November 2008

Keywords:
Respiratory supercomplex
Respiratory string
Electron microscopy
Single particle analysis

ABSTRACT

The individual protein complexes of the oxidative phosphorylation system (OXPHOS complexes I to V) specifically interact and form defined supramolecular structures, the so-called "respiratory supercomplexes". Some supercomplexes appear to associate into larger structures, or megacomplexes, such as a string of dimeric ATP synthase (complex V_2). A row-like organization of OXPHOS complexes I, III and IV into respiratory strings has also been proposed. These transient strings cannot be purified after detergent solubilization. Hence the shape and composition of the respiratory string was approached by an extensive structural characterization of all its possible building blocks, which are the supercomplexes. About 400,000 molecular projections of supercomplexes from potato mitochondria were processed by single particle electron microscopy. We obtained two-dimensional projection maps of at least five different supercomplexes, including the supercomplex $I+III_2$, III_2+IV_1, V_2, $I+III_2+IV_1$ and I_2+III_2 in different types of position. From these maps the relative position of the individual complexes in the largest unit, the $I_2+III_2+IV_2$ supercomplex, could be determined in a coherent way. The maps also show that the $I+III_2+IV_1$ supercomplex, or respirasome, differs from its counterpart in bovine mitochondria. The new structural features allow us to propose a consistent model of the respiratory string, composed of repeating $I_2+III_2+IV_2$ units, which is in agreement with dimensions observed in former freeze-fracture electron microscopy data.

1. Introduction

Many processes in the cell require energy which can be stored in a chemical way. Adenosine triphosphate (ATP) is such a storage molecule. Hydrolysis of ATP produces besides inorganic phosphate and adenosine diphosphate (ADP) "free energy" which can be used to drive energy-requiring processes. The main eukaryotic cell compartment for ATP production is the mitochondrion, where energy of oxidation is coupled with the formation of ATP. This is performed by ATP synthase which utilizes an electrochemical gradient of protons created by three respiratory protein complexes (NADH dehydrogenase — complex I, dimeric cytochrome *c* reductase — complex III_2, cytochrome *c* oxidase — complex IV) across the inner mitochondrial membrane. Proton translocation depends on the transfer of electrons from NADH or $FADH_2$ through complex I, III, IV and succinate dehydrogenase (complex II) to oxygen which is reduced into water. Electron flow between the complexes is mediated by two mobile electron carriers, ubiquinone and cytochrome *c*, which are located in the inner membrane and the intermembrane space, respectively [1]. Nowadays, availability of high-resolution structures of complex II, III, and IV (reviewed in [2]), the hydrophilic arm of complex I [3] and most of the complex V (or ATP synthase) subunits [4–7] gives more detailed insight into the function of individual complexes in mitochondrial respiration.

A pioneering electron microscopy (EM) study of the freeze-fractured and deep-etched inner mitochondrial membranes from *Paramecium multimicronucleatum* revealed at least two types of repeating structures in the membrane and thereby gave the first indication of an ordered organization of respiratory complexes in the membrane [5]. The first periodic structure, a double row of particles following the full length of the outer curve of helically shaped tubular cristae, was identified as ribbons of dimeric ATP synthase. In another study, rows of ATP synthase particles were visualized by cryo-electron tomography of *Neurospora* mitochondria [8]. Recently, a tomographic analysis of the inner mitochondrial membrane from bovine mitochondria showed the structure of these ribbons of dimeric ATP synthase in greater detail [9]. The second type of non-random arranged complexes, consisting of large 13×22 nm particles with a spacing of 26–30 nm, was interpreted as rows of dimeric complex I [10], but has not been confirmed by other structural investigations.

Presence of such periodic structures in the inner membrane presumes a specific association between single respiratory complexes. Indeed, Schägger and Pfeiffer [11] showed that a mild solubilization of

* Corresponding authors. Tel.: +31 50 3634225; fax: +31 50 3634800.
E-mail addresses: e.j.boekema@rug.nl (E.J. Boekema), r.kouril@rug.nl (R. Kouřil).

0005-2728/$ – see front matter © 2008 Elsevier B.V. All rights reserved.
doi:10.1016/j.bbabio.2008.10.010

the inner mitochondrial membrane from yeast and bovine heart mitochondria followed by Blue-native PAGE (BN-PAGE) led to a separation of high-molecular bands with a mass between ~1.2 MDa and ~3 MDa, which were identified as specific supercomplexes of individual respiratory complexes. Using a similar biochemical approach, different types of respiratory supercomplexes were subsequently identified in many other organisms (reviewed in [11–14]). These supercomplexes are formed by two to three different respiratory complexes with up to four copies, with the following composition: I_2+III_2, $I+III_2$, I+IV, III_2+IV_{1-2} and $I+III_2+IV_{1-4}$. The latter supercomplex has been named respirasome [11]. In addition, dimers have been found for complexes I (I_2) and V (V_2). The dimeric forms of mitochondrial complex I and V seem to be a special type of association for this organelle, because these enzymes are monomeric in, for instance, plant chloroplasts and all eubacteria.

The structural characterization of respiratory supercomplexes is a prerequisite for our understanding of their functioning but also for the higher organization of supercomplexes in the inner membrane. Experimental data indicate that formation of supercomplexes allows enhanced electron transfer rates (electron channeling) and increases the stability of individual OXPHOS complexes. The higher organization of supercomplexes seems to be important for the morphology of the inner mitochondrial membrane and an increase of the protein insertion capacity of the inner mitochondrial membrane (reviewed in [15]). Single particle EM and image analysis revealed two-dimensional projection maps of plant supercomplex $I+III_2$ [16,17], dimeric ATP-synthase [18,19], yeast supercomplex III_2+IV_{1-2} [20] and bovine $I+III_2+IV$ supercomplex [21]. Recently, the first three-dimensional structure of bovine respirasome was solved by EM and the arrangement of the individual complexes within this supercomplex was suggested [22]. The resolution of this 3D map is, however, still too low to precisely position the smallest of the components, complex IV. Structural work on the dimeric complex V indicated that this supercomplex is kinked in its membrane-embedded parts, leading to a strong local curvature of the membrane [18]. This suggests that the dimeric ATP synthase is involved in shaping the inner mitochondrial membrane folding. So far, there is no direct structural evidence for the existence of a supercomplex containing a dimer of complex I, and finally, complex II appears not to be incorporated in any type of supercomplex.

The existence of defined types of supercomplexes is now well established, but since the various oxidative phosphorylation (OXPHOS) complexes differ in abundance they are considered to not completely form part of supermolecular structures. Rather, OXPHOS supercomplexes and singular OXPHOS complexes co-exist within the inner mitochondrial membrane. On the other hand, it is also likely that higher types of organization exist in many organisms. The string-like bovine megacomplex consisting of ATP synthase dimers [9], discussed above, is one specific structure. Based on biochemical data, another megacomplex has been proposed, which was called the respiratory string. It was suggested, that $I+III_2+IV_4$ supercomplexes are interconnected with the III_2+IV_4 supercomplex [14]. This suggestion was based on the earlier observations in freeze-fractured electron microscopy specimens [10]. However, considering the known size of the individual complexes, the proposed model cannot explain the observed periodic spacing of 26–30 nm.

The goal of the present study was a structural characterization of the higher organization of respiratory supercomplexes into rows or respiratory strings in the inner membrane. Potato mitochondria were chosen as a study target. An important reason to use potato mitochondria is the fact that a supercomplex containing two copies of complex I was detected by BN-PAGE [23]. Because a transient megacomplex such as the hypothetical respiratory string is probably impossible to purify after detergent solubilization we decided to approach the problem by an extensive characterization with single particle electron microscopy of all the possible building blocks of periodic structures. About 400,000 projections of supercomplexes were processed. We obtained two-dimensional projection maps of at least five different supercomplexes, including the supercomplex $I+III_2$, III_2+IV_1, V_2, $I+III_2+IV_1$ and I_2+III_2 in different types of position. From these maps the relative position of the individual complexes could be determined in a consistent way. These new structural features allow us to propose a refined model of a respiratory string, which is also in agreement with former freeze-fracture EM data [10].

2. Material and methods

2.1. Preparation of mitochondria

Freshly harvested potato tubers (*Solanum tuberosum* var. cilena) were purchased from a local farmer and stored at 4 °C. Mitochondria were prepared by homogenizing 200 g of plant material at 4 °C using a Waring blender for 3×5 s, filtrated through four layers of muslin. Subsequently, organelles were purified by differential centrifugations and Percoll density gradient centrifugation as outlined previously [24]. Isolated mitochondria were either directly analyzed by gel electrophoresis or stored at minus 80 °C.

2.2. Purification and characterization of respiratory supercomplexes

The mitochondrial inner membrane-protein complexes of potato were solubilized using a buffer with 5% digitonin, 30 mM HEPES, 150 mM K-acetate, 10% glycerine, pH 7.4. To characterize solubilized respiratory supercomplexes, protein solution was firstly separated by one-dimensional Blue-native (BN) PAGE [25]. Secondly, to establish the subunit content, gel strips including the resolved protein complexes were placed horizontally onto a second gel dimension which was carried out in the presence of SDS (two-dimensional BN/SDS PAGE). Afterwards, the gels were stained with Coomassie-Blue.

To purify respiratory supercomplexes, solubilized complexes were loaded on a 0.3–1.5 M sucrose gradient containing 15 mM Tris base, pH 7.0, 20 mM KCl, 0.2% digitonin and separated by ultracentrifugation (17 h at 150,000× *g* and 4 °C). Afterwards, the gradients were fractionated and the fractions were examined for protein complexes by one-dimensional BN/SDS PAGE and Coomassie-Blue staining. In some cases, bands from a one-dimensional BN-PAGE gel were cut out and the protein complexes were electro-eluted with elution buffer (25 mM Tricine, 7.5 mM Bis–Tris and 0.01% digitonin) at 4 °C [24]. Intactness of electro-eluted protein complexes was checked using another one-dimensional BN-PAGE.

2.3. Electron microscopy and single particle analysis

Selected fractions of the sucrose gradient were dialyzed against buffer (15 mM Tris/HCl, 20 mM KCl and 0.2% digitonin) to decrease the sucrose content and to improve a quality of EM specimen. Electro eluted protein complexes were directly used for specimen preparation without any further treatment. Negatively stained specimens were prepared with 2% uranyl acetate on glow-discharged carbon-coated copper grids. Electron microscopy was performed on a Philips CM120 electron microscope equipped with a LaB6 tip operating at 120 kV. Images were recorded with a Gatan 4000 SP 4K slow-scan CCD camera at 80,000× magnification at a pixel size (after binning the images) of 0.375 nm at the specimen level with GRACE software for semi-automated specimen selection and data acquisition [26]. Single particle projections were selected from micrographs both by hand and reference-based automated particle selection procedure incorporated into GRIP (GRoningen Image Processing) software. Single particle data sets were analyzed with the GRIP software on a PC-cluster, including multi-reference and no-reference alignments, multivariate statistical analysis, and hierarchical ascendant classification [27]. Final two-dimensional projection maps were calculated

from the best resolved classes, by summing only the best 5–20% of the projections, with the correlation coefficient determined in the alignment step as a criterion.

3. Results

3.1. Purification and characterization of respiratory supercomplexes

Solubilization of isolated potato mitochondria by digitonin and analysis of the solubilized protein complexes by two-dimensional BN/SDS PAGE allowed identification of the respiratory supercomplexes present in potato mitochondria (Fig. 1). In line with previous results [23,28], significant numbers of supercomplexes comprising of complexes I, III and IV (III_2+IV, I+III_2, I_2+III_2 and I+III_2+IV) along with dimeric ATP synthase and the five individual complexes were detected.

For single particle EM analysis, solubilized respiratory supercomplexes were purified by sucrose density gradient ultracentrifugation. The gradient was subsequently fractionated and small aliquots of the fractions were analyzed by BN-PAGE to monitor their protein complex composition (Fig. 2A). Fractions enriched in specific respiratory supercomplexes were used for single particle EM analysis. If necessary, either described purification approach was repeated several times to obtain a fraction with a sufficient concentration of specific supercomplex or projections of specific supercomplex found in different sucrose gradient fractions were combined to obtain a data set with a sufficient number of projections suitable for single particle image analysis. Alternatively, EM analysis was performed on electro-eluted supercomplexes from a one-dimensional PAGE strip. To confirm the intactness of the supercomplex after electro-elution, small aliquots of the electro-eluted supercomplexes were analyzed again with one-dimensional BN-PAGE (Fig. 2B).

3.2. Structural analysis of complex I

Single particle EM and image analysis of sucrose gradient fraction enriched in content of complex I revealed a top-view and several types of side-view projections of complex I (Fig. 3). Averaged projection map of the top-view of the complex I clearly indicate that the membrane part of the complex I is characteristically curved (Fig. 3A). Side-view projections of complex I were resolved for two different orientations of complex I on the support carbon film (Fig. 3B–F). More detailed comparison of side-view projections indicates that the main differences are in the structure of the hydrophilic arm (compare Fig. 3C, D vs. B, E, F), although small differences in the membrane part are present as well. As the membrane part of the complex I in Fig. 3C and D appears to be more bended compared to the other side-view projections (Fig. 3B, E, F), different structural features of the hydrophilic arms can reflect a different orientation of complex I on the carbon support film. The reason for the slightly different orientation of complex I can be either in flexibility or contrary conformation of the hydrophilic arm, which can, subsequently, lead to distinct positions of the complex on the carbon film. The carbonic anhydrase domain, which was found to be tightly associated with the membrane part of green plant complex I

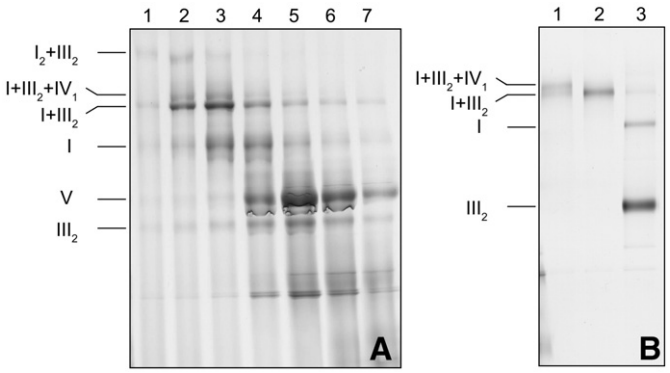

Fig. 2. Preparation of mitochondrial OXPHOS supercomplexes from potato for EM analyses. Protein complexes of potato mitochondria were either separated by sucrose gradient ultracentrifugation or by one-dimensional Blue-native PAGE and subsequent electro-elution. (A) Aliquots of fractions of the sucrose gradient were resolved by one-dimensional Blue native PAGE to monitor the protein complex composition of the fractions. (B) Aliquots of electro-eluted I+III_2+IV supercomplex (lane 1), I+III_2 supercomplex (lane 2) and complex III_2 (lane 3) were reanalyzed by one-dimensional Blue native PAGE to monitor purity of the fractions. Identities of the resolved protein complexes are indicated to the left of the gels (for designations see Fig. 1).

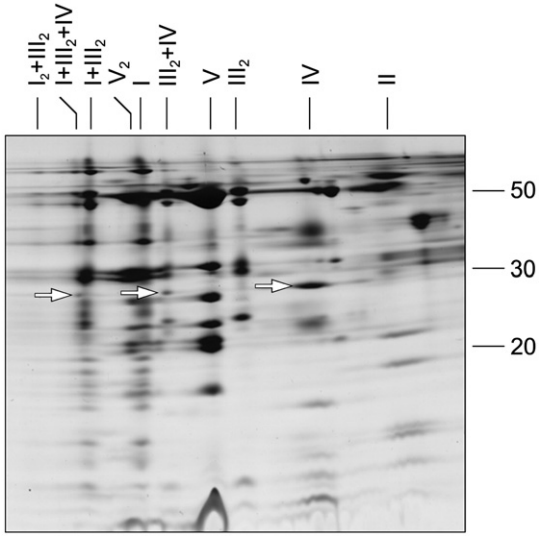

Fig. 1. Analyses of protein complexes of potato mitochondria by two-dimensional Blue native/SDS PAGE. Molecular masses of standard proteins are given to the right of the gel (in kDa). Designations: I, II, IV, V: monomeric complexes I, II, IV, V; III_2, V_2: dimeric complexes III, V; III_2+IV: supercomplex formed of dimeric complex III and monomeric complex IV; I+III_2: supercomplex formed of complex I and dimeric complex III; I_2+III_2: supercomplex formed by dimeric complex III and two copies of monomeric complex I; I+III_2+IV: supercomplex formed of complex I, dimeric complex III and complex IV. The white arrow indicates the Cox II subunit of complex IV, which forms part of (i) complex IV, (ii) of the III_2+IV supercomplex and (iii) of the I+III_2+IV supercomplex.

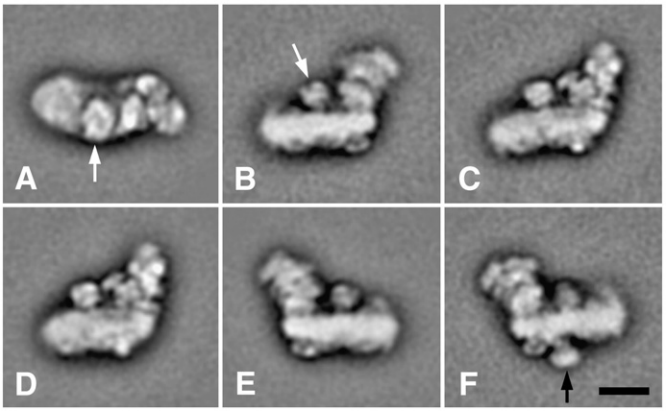

Fig. 3. Single particle electron microscopy of the complex I from potato mitochondria. Projection map (A) represents the top-view of the complex I. (B–F) show side-view projections of the complex I with different orientations on the support carbon film, respectively. Carbonic anhydrase domain (a white arrow), which associates to complex I in plant mitochondria, is clearly resolved in all presented projections. An unknown density attached to the membrane part of complex I was revealed in some side-view projections as indicated by a black arrow in (F). Projection maps (A–F) are averaged class sums of 454, 276, 241, 516, 634, and 314 aligned particles, respectively. The scale bar equals to 10 nm.

[16,17,29], can also be recognized in our projection maps. Moreover, the trimeric arrangement of carbonic anhydrase domain was clearly resolved in some projection maps (Fig. 3D, E). Appearance of carbonic anhydrase showing its trimeric structure in the side-view projections evidently indicates its flexible attachment to the membrane part of complex I. The flexibility of the carbonic anhydrase domain is probably located in a flexible connection between the trimeric moiety and the membrane anchor.

Interestingly, one class of the side-view projections of complex I reveals a novel density of unknown composition, which is attached to the membrane part of the complex I, approximately on the opposite side of the carbonic anhydrase (Fig. 3F). Estimated from its size, which is slightly smaller than the carbonic anhydrase domain of 75 kDa, it could have a mass between 40 and 60 kDa.

3.3. Structural analysis of the I+III_2 supercomplex

The projection maps in Fig. 4 show the results of single particle EM and image analysis of sucrose gradient fractions enriched in the potato I+III_2 supercomplex. Top-view projections revealed a typical U-shaped feature of the I+III_2 supercomplex (including the density of the carbonic anhydrase domain) which were observed before in other plant species (Fig. 4A–C) [16,17,29]. Detailed inspection of resolved classes shows that some represent the I+III_2 supercomplex in a more opened conformation (Fig. 4A) compared to others (Fig. 4B and C). In addition, the carbonic anhydrase domain, attached in the center of the membrane arm of complex I, is distinguishable in some top-view projections as the most stain-excluding density (e.g. arrow, Fig. 4A). Fig. 4D–F represents two different side-view projections of the I+III_2 supercomplex, which clearly depict typical features of the hydrophilic arm of complex I and the dimeric complex III. The carbonic anhydrase domain can be distinguished only under a certain angular view (arrow, Fig. 4E). In the other two side-views, the angular position is such that the density of the carbonic anhydrase is less recognizable as it merges with densities of either the membrane-protruding part of complex III_2 (Fig. 4D) or the hydrophilic arm of complex I (Fig. 4F). Besides top- and side-view projections, several classes with tilted supercomplex I+III_2 views were found (Fig. 4G–I). Assignment of complex I in the tilted view projections was facilitated by localization of the trimeric density of the carbonic anhydrase domain, which is composed by three subunits, on the hydrophilic arm of the complex I (Fig. 4G–I). They correspond to the projection densities of singular complex I at a similar angular view (Fig. 4J). The typical feet-like features and characteristic shape of membrane-protruding part of complex III_2 are recognizable in the right-bottom part of the projection maps (Fig. 4G–I).

3.4. Structural analysis of I_2+III_2 and I+III_2+IV supercomplexes

Biochemical analysis indicated the presence of large supercomplexes in some sucrose gradient fractions, like the I_2+III_2 and I+III_2+IV supercomplex (Fig. 2A). Single particle EM and image analysis of these fractions revealed, indeed, the presence of large particles, although their abundance was rather low, with about 1–2 copies per EM micrograph. Fig. 5A shows a class average of one type of such a large particle, which was assigned to a side-view projection of the I_2+III_2 supercomplex. The center of the projection map can be unambiguously assigned to the dimer of complex III, mainly due to its typical feature of the membrane-protruding part. Complex III_2 is symmetrically flanked by two copies of complex I, whose hydrophilic arms are recognizable. Image analysis revealed that in some cases the complex I at the right-side of complex III_2 is incomplete in the hydrophilic arm (Fig. 5B). Importantly, the incompleteness of the I_2+III_2 supercomplex does not lead to a different orientation of the particle on the carbon support film and both the complete I_2+III_2 supercomplex and the fragment reveal the same features in resolved projection maps (compare Fig. 5A and B).

Fig. 5C shows a class average, which brings to light substantial different features of the complex III_2 compared to its corresponding density in the complete/incomplete I_2+III_2 supercomplex (Fig. 5A, B). Due to the strong similarity of projection map in Fig. 5C with the side-view projection of the I+III_2 supercomplex (4F), we suggest that the projection map in Fig. 5C represents the side-view of the I+III_2 supercomplex with an extra mass attached on the right side of the supercomplex. Furthermore, the similarity indicates that the extra mass has to represent a protein of a smaller size than e.g. the hydrophobic arm of complex I, as there is a minimal influence of the extra mass on the side-view orientation of the I+III_2 supercomplex on the carbon support film. Fig. 5D shows a class average, which represents a well-recognizable top-view projection of the I+III_2 supercomplex with an extra density attached close to the complex III along the interaction interface between complex I and complex III. Based on the biochemical analysis of sucrose gradient fractions (Fig. 2A) and the size of the extra mass, we suggest that this density represents complex IV and projection maps in Fig. 5C and D represent the side- and top-view of the I+III_2+IV supercomplex, respectively. This supercomplex represents the largest individual unit in OXPHOS. It has been found previously in bovine mitochondria and was named the respirasome [11].

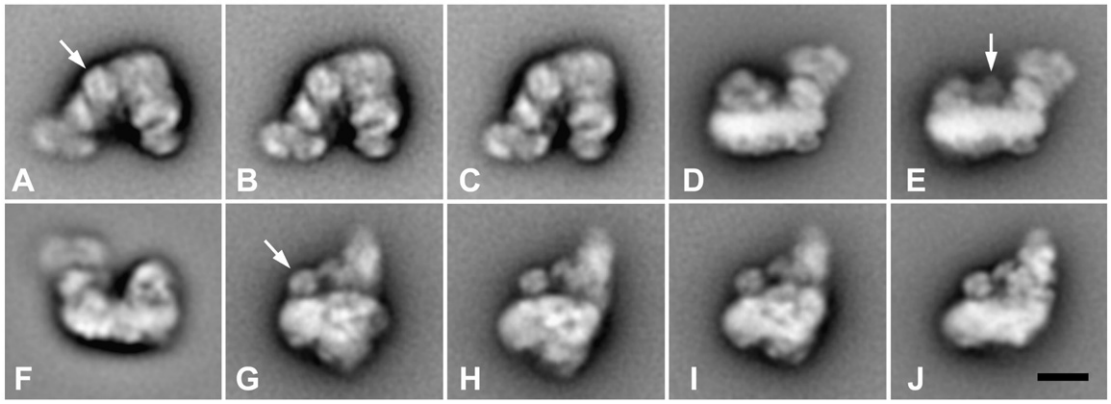

Fig. 4. Single particle electron microscopy of the I+III_2 supercomplex from potato mitochondria. Projection maps (A–C) represents top-view projections of the I+III_2 supercomplex in a more open (A), intermediate (B) and close conformation (C). (D–F) depict side-view projections of the I+III_2 supercomplex with different orientations on the support carbon film. Projections (G–I) show tilted views of the I+III_2 supercomplex. Projection map (J) represents complex I with a similar orientation on the support carbon film like in case of tilted views of the I+III_2 supercomplex shown in (G–I). Projection maps (A–J) are averaged class sums of 1422, 924, 1320, 1024, 1024, 1500, 512, 512, 512 and 1500 aligned particles, respectively. The carbonic anhydrase is indicated by white arrows in (A), (E), and (G). The scale bar equals to 10 nm.

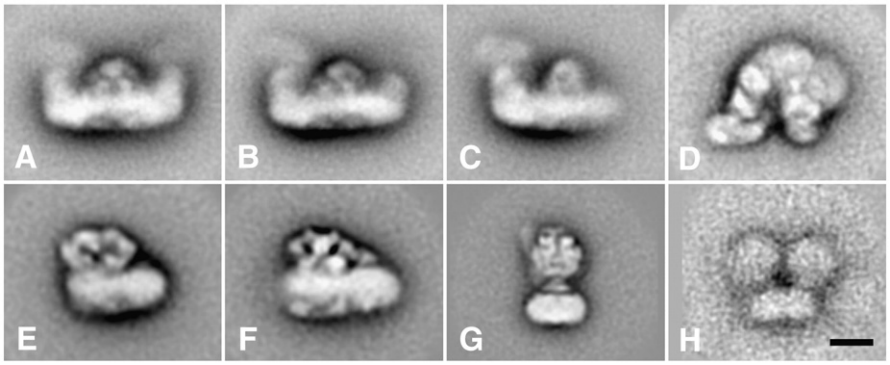

Fig. 5. Single particle electron microscopy of the I_2+III_2, $I+III_2+IV$, III_2+IV, V, and V_2 supercomplexes from potato mitochondria. Projection map (A) represents the side-view of the I_2+III_2 supercomplex whereas (B) shows the same supercomplex lacking parts of the NADH-oxidizing domain in one copy of complex I. Projection map (C) represents a side-view of the $I+III_2+IV$ supercomplex, (D) represents the top-view of the $I+III_2+IV$ supercomplex. (E) represents a side-view of supercomplex III_2+IV_1. Projection maps (F) represents, for comparison, potato's counterpart of supercomplex III_2+IV_1 found in yeast [20]. (G) and (H) represent the side-view projections of either monomeric or dimeric ATP synthase, respectively. Projection maps (A–H) are averaged class sums of 512, 512, 512, 238, 1024, 768, 642, and 50 aligned particles, respectively. The scale bar equals to 10 nm.

3.5. Structural analysis of the III_2+IV supercomplex and complex V

To prove the existence of a specific association between complex III and complex IV, we performed single particle EM analysis of the III_2+IV supercomplex. Compared to yeast mitochondria, abundance of this supercomplex is rather low, possibly reflecting a weaker association of the two involved OXPHOS complexes. Due to its low abundance in sucrose gradient fractions, we analyzed the III_2+IV supercomplex from an electro-eluted one-dimensional BN-PAGE band. Fig. 5E shows a side-view projection map of the III_2+IV supercomplex, which reveals a specific association between complex III_2 and one copy of complex IV. The overall structure of the side-view projection of the potato supercomplex III_2+IV is similar to the one found in yeast [20] (Fig. 5F), but their precise comparison is difficult due to a lower resolution of the potato projection map. In addition to the III_2+IV supercomplex, single particle EM analysis revealed side-view projections of monomeric ATP synthase (complex V) and few copies of dimeric ATP synthase (V_2) in electro-eluted fraction (Fig. 5G and H). The structure of monomeric complex V revealed the F_0 and F_1 part as well as the stalk. Although the resolution of dimeric ATP synthase is very low, the obtained projection map indicates a small angle between associated monomers.

4. Discussion

The existence of a higher organization of respiratory complexes into rows or respiratory strings was indicated in intact mitochondria by both freeze-fracture EM studies and electron tomography experiments [8–10]. The data showing the linear association of dimeric ATP synthase (complex V_2) are convincing because the bulky F_1 parts with a diameter of 10 nm protrude from the membrane [9], but the structure and/or composition of the respiratory string is not clear. Purified strings might give an answer, but even under mild solubilization conditions the respiratory strings are disrupted and isolated supercomplexes represent just their fragments. In the end, structural characterization of these fragments could allow us to reconstruct the respiratory string. In this study, we performed an extensive structural characterization of respiratory supercomplexes (I_2+III_2, $I+III_2+IV_1$, $I+III_2$, III_2+IV_1, V_2) and singular complexes (complex I and V) isolated from one organism where a higher organization into a respiratory string is expected to be present, based on a BN-PAGE survey. Because about 400,000 projections were analyzed, we are quite confident that all the supercomplex structures which are relevant for a higher type of organization into mega-complexes or respiratory strings have been detected. The final projection maps shown here, however, only represent a fraction of the data set. Many other maps, omitted here because of their redundancy, mostly differ slightly in orientation of supercomplexes or in quality of preserved details.

Single particle EM analysis of both sucrose gradient and electro-eluted fractions indicates that a singular complex I and the $I+III_2$ supercomplex were the most abundant particles. Abundance of the I_2+III_2 supercomplex and supercomplexes containing complex IV was substantially lower. Indeed, former biochemical analysis indicates that (i) the I_2+III_2 supercomplex only becomes visible upon prolonged staining of BN gels and (ii) only about 10% of complex IV is part of the $I+III_2+IV_{1-4}$ and III_2+IV_{1-2} supercomplexes, when the rest of complex IV is in monomeric state under the conditions applied [28].

Projection maps of complex I revealed, beside the detailed features of both the trimeric carbonic anhydrase domain and the hydrophilic arm, a characteristic curvature of the membrane arm of the complex as it is evident from the top-view projection (Fig. 3). The same curvature of the membrane arm of complex I was observed in the 3D structure of complex I from *Yarrowia lipolytica* [30] and 2D crystals of the membrane arm of complex I from *Escherichia coli* [31]. Based on the curved feature of the membrane arm of complex I we could unambiguously assign the handedness of our 2D projection maps defining the top-view projection as the view from the matrix site. It is worth mentioning that the top-view projection of complex I (Fig. 3A) does not exactly represent the view perpendicular to the membrane plane. It can be derived from the stain distribution along the membrane arm of complex I that the viewing angle in this projection is about 10° off from being perpendicular. In accordance with previous results, side-view projections of complex I revealed the membrane-protruding densities at both ends of complex I membrane arm (Fig. 3B–F) [29,30]. Interestingly, a novel density was resolved on the intermembrane site of the complex I (Fig. 3F). The extra domain is attached to the complex I membrane arm, approximately at the opposite side of the carbonic anhydrase domain. Complex I particles with this extra domain were not detected in any other plant or animal species. At this moment we cannot assign its composition, but given the size it seems to represent a plant specific protein which is slightly smaller than trimeric carbonic anhydrase with a mass around 40–60 kDa.

Image analysis of the second most abundant supercomplex, the $I+III_2$ supercomplex, revealed different top-, side- and tilted view projections (Fig. 4). Top-view projections of the $I+III_2$ supercomplex indicate the same curvature of the complex I membrane arm, as in the case of singular complex I. In all resolved projections, complex III_2 was found to associate with complex I exclusively at the inner part of the curved membrane arm (Fig. 4A–C, Fig. 6). An angular difference

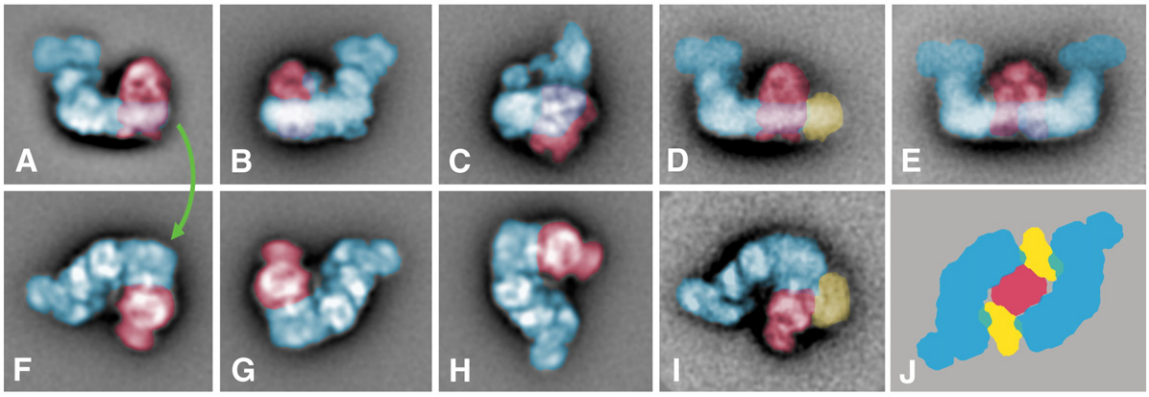

Fig. 6. A schematic assignment of different side-views of the I+III_2 (A–C), I+III_2+IV (D), and I_2+III_2 (E) supercomplexes. Green arrow illustrates horizontal flips from side-view projections (A–E) to corresponding top-view projections (F–I). (J) represents a proposed model of a top-view projection of the I_2+III_2+IV_2 supercomplex. Note that the frame of 6I shows half of this structure, but in a slightly tilted position out of the membrane plane. Complex I is depicted in blue, complex III in red, and complex IV in yellow.

between the membrane arm of complex I and complex III_2 indicates an apparent flexibility of their association (Fig. 4A–C), which can be important in vivo, where the individual complexes associate in the heavily folded mitochondrial inner membrane together with other components. As in the case of the top-view projection of singular complex I, the top-view projection of the I+III_2 supercomplex also represents an angular view (~10° tilt out of the membrane plane). This can be evaluated from the amount of deviation from 2-fold symmetry, expected in the projection of dimeric complex III without tilt. Unambiguous assignment of the side- and tilted views of the I+III_2 supercomplex could be derived from the top-view projection of the supercomplex (Fig. 6A–C, F–H). Recognition of characteristic features of complex III_2 in both side- and tilted view projections of the I+III_2 supercomplex gives us insights into the way dimeric complex III associates to complex I.

Fig. 5C and D represent a side- and top-view projection map, which are, except of the presence of a small extra mass, similar to the maps of corresponding views of the I+III_2 supercomplex (Fig. 4F, A, respectively). Based on a biochemical characterization of sucrose gradient fractions and dimensions of the extra density, this extra mass was assigned to complex IV and the whole projection map to supercomplex I+III_2+IV, the respirasome (Fig. 6D, I). The top-view projection of the respirasome indicates that the complex IV associates to both complex I and III (Fig. 6I). The resolved projection map of the III_2+IV supercomplex clearly indicates a stable association between these two complexes (Fig. 5E). However, due to the low resolution of the III_2+IV supercomplex it is not possible to determine which site of complex IV is involved in the interaction with complex III_2. Since the overall shape of the supercomplex III_2+IV projection map from potato is rather similar to that of the yeast III_2+IV_1 supercomplex, we assume that potato complex III_2 and complex IV associate in a similar way like in the yeast supercomplex III_2+IV [20].

Our data indicate that the structure of the potato respirasome differs from the 3D model of the bovine respirasome [22]. The proposed model for the bovine respirasome suggests that (i) complex III_2 associates to complex I from the site, which is opposite to the binding site we found in potato, (ii) complex IV is attached at the end of the membrane arm of complex I, whereas in potato respirasome complex IV associates with complex III_2. So far, neither biochemical data nor single particle EM analysis gave evidence of the existence of the I+IV supercomplex in potato mitochondria, at least under conditions applied in our experiments.

Potato mitochondria are special for I_2+III_2 supercomplexes, although these particles are not very abundant in detergent solubilized membrane fractions. Sucrose gradient fractions where at least trace amounts of the I_2+III_2 supercomplexes were detected by one-dimensional BN-PAGE (Fig. 2A), were subjected to an extensive single particle EM analysis. Fig. 5A shows, for the first time, a side-view projection map of this supercomplex. The middle part of the projection map clearly shows symmetric features, which could be unambiguously assigned to the dimeric complex III. The densities which represent both hydrophilic arms of the two complex I moieties are faint, or even absent on the right position in Fig. 5B. This can be explained by the dissection of the upper part of the hydrophilic arm, which was also observed in complex I from other species [16]. Moreover, the faint appearance is also a matter of stain embedding. Fig. 6J shows a schematic top-view of the I_2+III_2+IV_2 supercomplex. This indicates that in the side-view position one of the membrane arms is over 20 nm away from the carbon support film.

The side-view map of the I_2+III_2 supercomplex likely also includes two copies of complex IV but because of potentially overlapping positions their presence cannot be ascertained. Together with the top- and side-view maps of the I+III_2+IV supercomplex we can now deduce the relative positions in the full I_2+III_2+IV_2 supercomplex, of which we did not observe substantial numbers of top-view projections (Fig. 6J) and complete the assignment of the largest possible supercomplex, as deduced from 400,000 potential fragments.

Based on our 2D projection maps of potato supercomplexes we suggest a megacomplex organization in the inner mitochondrial membrane, which was previously named the respiratory string (Fig. 7). We propose that a central role is given to dimeric complex III which is able to bind up to two copies of complex I. Complex IV is supposed to play a role in connection of the I_2+III_2 supercomplexes, and probably also in clasping the flexible interaction between I_2+III_2 supercomplexes. Although EM analysis only revealed a stable association between complex III_2 and one copy of complex IV, binding of two complex IV molecules can be expected, due to the dimeric structure of the complex III. Moreover, biochemical data indicate that the I+III_2 supercomplex can associate with up to 4 copies of complex IV giving the I+III_2+IV_{1-4} supercomplexes [28]. The fact that these complexes have not been found in this extensive search may indicate that they easily dissociate upon negative staining procedure used in the EM analysis. In the proposed model, the I_2+III_2+IV_2 supercomplex represents the basic building block (Fig. 7). These supercomplexes form a string by the interaction of two copies of complex IV, whereby each supercomplex contributes one molecule. This organization is based on (i), the first structure of supercomplex I_2+III_2 which shows that dimeric complex III can bind two copies of complex I, (ii), the structure of supercomplex I+III_2 and (ii), the structure of the III_2+IV supercomplex. Although we were not able to visualize the III_2+IV_2 supercomplex, this supercomplex was present in one-dimensional BN-PAGE gels, making it likely that the potato structure is similar to that found in yeast [20].

Previous model of string architecture of respiratory chain supercomplexes in bovine mitochondria differs from our model, because

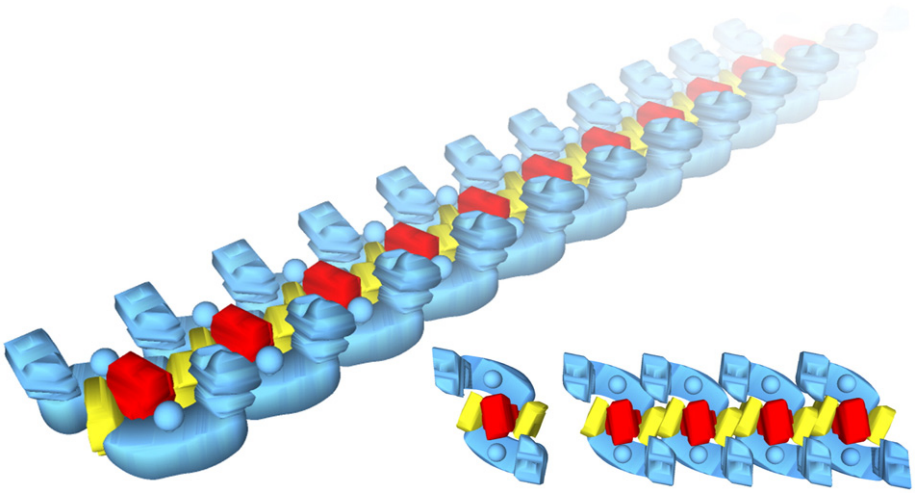

Fig. 7. A schematic model on scale of the organization of respiratory chain complexes into respiratory string. The basic unit consists of two copies of complex I (blue), one copy of complex III_2 (red), and two copies of complex IV (yellow). Association of basic units into a string is mediated by complex IV, which interacts with a neighboring complex IV through a dimeric interface found in the X-ray structure [33]. The model was created using a free version of Google SketchUp software.

the former is based on binding of only one copy of complex I to dimeric complex III [14]. Indeed, supercomplexes including more than one copy of complex I were not observed in beef. Further, the ratio of complexes I, III and IV in our model is 1:1:1 and differs from the previous reported ratio of 1:3:6. [32]. However, one has to realize that the 1:3:6 ratio reflects the total concentration of each complex in the inner mitochondrial membrane including the free complexes. The $I_2+III_2+IV_2$ repeating motif in the model proposed for potato measures about 26 nm (going from one centre of complex III_2 to the next) which is comparable to the earlier observed spacing of 26–30 nm by freeze-fractured EM [10]. Wittig et al. pointed out that this distance equals the length of three repeating units of supercomplexes III_2+IV_2 (see Fig. 3 in [14]). This, however, cannot be the case for potato since the length of one III_2+IV_2 supercomplex measured in the configuration $IV+III_2+IV$ equals already 26 nm [20]. Therefore, it is unlikely that two neighboring complex III_2 are separated by two dimers of complex IV because addition of two copies of complex IV to the III_2+IV_2 complex would increase the width by about 10 nm to a final 36 nm. Presently it cannot be decided whether the string architecture is conserved in eukaryotes or rather differs in different organisms.

In conclusion, the data presented here give the first structural insight in a respiratory string from mitochondria, although in an indirect way, based on the structural characterization of supercomplexes obtained after detergent disruption of the mitochondrial inner membrane. A final proof is in theory possible by electron tomography on ice embedded mitochondria, in a way as performed to visualize the ATP synthase strings [9]. Tomography, however, has a much lower resolution than single particle analysis. The resolution is around 6–8 nm in the case of large objects such a mitochondrion. In contrast, single particle analysis typically provides information at 2 nm. Hence, present electron tomography can visualize the protruding headpieces of ATP synthase which have a diameter of 10 nm, but it cannot reveal the presence of many smaller membrane-embedded components such as complex IV, whose crucial role in the connection of the much larger dimeric complex III and complex I was suggested in our model of respiratory string.

Acknowledgements

We thank Dr. Wilko Keegstra (University of Groningen) for development of a reference-based automated particle selection procedure and Dagmar Lewejohann (Universität Hannover) for expert technical assistance. H.P.B. acknowledges grants of Deutsche Forschungsgemeinschaft (Br 1829-7/3 and Br 1829-8/1) and E.J.B. grants of the Dutch science foundation NWO-CW.

References

[1] M. Saraste, Oxidative phosphorylation at the fin de siecle, Science 283 (1999) 1488–1493.
[2] P.R. Rich, The molecular machinery of Keilin's respiratory chain, Biochem. Soc. Trans. 31 (2003) 1095–1105.
[3] L.A. Sazanov, P. Hinchliffe, Structure of the hydrophilic domain of respiratory complex I from *Thermus thermophilus*, Science 311 (2006) 1430–1436.
[4] J.P. Abrahams, A.G.W. Leslie, R. Lutter, J.E. Walker, Structure at 2.8-Angstrom resolution of F1-ATPase from bovine heart-mitochondria, Nature 370 (1994) 621–628.
[5] V.K. Dickson, J.A. Silvester, I.M. Fearnley, A.G.W. Leslie, J.E. Walker, On the structure of the stator of the mitochondrial ATP synthase, EMBO J. 25 (2006) 2911–2918.
[6] C. Gibbons, M.G. Montgomery, A.G.W. Leslie, J.E. Walker, The structure of the central stalk in bovine F-1-ATPase at 2.4 Angstrom resolution, Nature Struct. Biol. 7 (2000) 1055–1061.
[7] D. Stock, A.G.W. Leslie, J.E. Walker, Molecular architecture of the rotary motor in ATP synthase, Science 286 (1999) 1700–1705.
[8] D. Nicastro, A.S. Frangakis, D. Typke, W. Baumeister, Cryo-electron tomography of *Neurospora* mitochondria, J. Struct. Biol. 129 (2000) 48–56.
[9] M. Strauss, G. Höfhaus, R.R. Schröder, W. Kühlbrandt, Dimer ribbons of ATP synthase shape the inner mitochondrial membrane, EMBO J. 27 (2008) 1154–1160.
[10] R.D. Allen, C.C. Schroeder, A.K. Fok, An investigation of mitochondrial inner membranes by rapid-freeze deep-etch techniques, J. Cell Biol. 108 (1989) 2233–2240.
[11] H. Schägger, K. Pfeiffer, Supercomplexes in the respiratory chains of yeast and mammalian mitochondria, EMBO J. 19 (2000) 1777–1783.
[12] N.V. Dudkina, J. Heinemeyer, S. Sunderhaus, E.J. Boekema, H.P. Braun, Respiratory chain supercomplexes in the plant mitochondrial membrane, Trends Plant Sci. 11 (2006) 232–240.
[13] I. Marques, N.A. Dencher, A. Videira, F. Krause, Supramolecular organization of the respiratory chain in *Neurospora crassa* mitochondria, Euk. Cell 6 (2007) 2391–2405.
[14] I. Wittig, R. Carrozzo, F.M. Santorelli, H. Schägger, Supercomplexes and subcomplexes of mitochondrial oxidative phosphorylation, Biochim. Biophys. Acta 1757 (2006) 1066–1072.
[15] E.J. Boekema, H.P. Braun, Supramolecular structure of the mitochondrial oxidative phosphorylation system, J. Biol. Chem. 282 (2007) 1–4.
[16] N.V. Dudkina, H. Eubel, W. Keegstra, E.J. Boekema, H.P. Braun, Structure of a mitochondrial supercomplex formed by respiratory-chain complexes I and III, Proc. Natl. Acad. Sci. U. S. A. 102 (2005) 3225–3229.
[17] K. Peters, N.V. Dudkina, L. Jänsch, H.P. Braun, E.J. Boekema, A structural investigation of complex I and I+III2 supercomplex from *Zea mays* at 11–13 Angstrom resolution: assignment of the carbonic anhydrase domain and evidence for structural heterogeneity within complex I, Biochim. Biophys. Acta 1777 (2008) 84–93.
[18] N.V. Dudkina, J. Heinemeyer, W. Keegstra, E.J. Boekema, H.P. Braun, Structure of dimeric ATP synthase from mitochondria: an angular association of monomers induces the strong curvature of the inner membrane, FEBS Lett. 579 (2005) 5769–5772.

[19] F. Minauro-Sanmiguel, S. Wilkens, J.J. Garcia, Structure of dimeric mitochondrial ATP synthase: novel F-0 bridging features and the structural basis of mitochondrial cristae biogenesis, Proc. Natl. Acad. Sci. U. S. A. 102 (2005) 12356–12358.
[20] J. Heinemeyer, H.P. Braun, E.J. Boekema, R. Kouřil, A structural model of the cytochrome *c* reductase/oxidase supercomplex from yeast mitochondria, J. Biol. Chem. 282 (2007) 12240–12248.
[21] E. Schäfer, H. Seelert, N.H. Reifschneider, F. Krause, N.A. Dencher, J. Vonck, Architecture of active mammalian respiratory chain supercomplexes, J. Biol. Chem. 281 (2006) 15370–15375.
[22] E. Schäfer, N.A. Dencher, J. Vonck, D.N. Parcej, Three-dimensional structure of the respiratory chain supercomplex $I_1III_2IV_1$ from bovine heart mitochondria, Biochemistry 46 (2007) 12579–12585.
[23] H. Eubel, L. Jansch, H.P. Braun, New insights into the respiratory chain of plant mitochondria. Supercomplexes and a unique composition of complex II, Plant Physiol. 133 (2003) 274–286.
[24] H.P. Braun, U.K. Schmitz, Affinity purification of cytochrome-*c* reductase from potato mitochondria, Eur. J. Biochem. 208 (1992) 761–767.
[25] I. Wittig, H.P. Braun, H. Schagger, Blue native PAGE, Nature Protocols 1 (2006) 418–428.
[26] G.T. Oostergetel, W. Keegstra, A. Brisson, Automation of specimen selection and data acquisition for protein electron crystallography, Ultramicroscopy 74 (1998) 47–59.
[27] M. van Heel, B. Gowen, R. Matadeen, E.V. Orlova, R. Finn, T. Pape, D. Cohen, H. Stark, R. Schmidt, M. Schatz, A. Patwardhan, Single-particle electron cryo-microscopy: towards atomic resolution, Q. Rev. Biophys. 33 (2000) 307–369.
[28] H. Eubel, J. Heinemeyer, H.P. Braun, Identification and characterization of respirasomes in potato mitochondria, Plant Physiol. 134 (2004) 1450–1459.
[29] S. Sunderhaus, N.V. Dudkina, L. Jänsch, J. Klodmann, J. Heinemeyer, M. Perales, E. Zabaleta, E.J. Boekema, H.P. Braun, Carbonic anhydrase subunits form a matrix-exposed domain attached to the membrane arm of mitochondrial complex I in plants, J. Biol. Chem. 281 (2006) 6482–6488.
[30] M. Radermacher, T. Ruiz, T. Clason, S. Benjamin, U. Brandt, V. Zickermann, The three-dimensional structure of complex I from *Yarrowia lipolytica*: a highly dynamic enzyme, J. Struct. Biol. 154 (2006) 269–279.
[31] E.A. Baranova, P.J. Holt, L.A. Sazanov, Projection structure of the membrane domain of *Escherichia coli* respiratory complex I at 8 Angstrom resolution, J. Mol. Biol. 366 (2007) 140–154.
[32] H. Schägger, K. Pfeiffer, The ratio of oxidative phosphorylation complexes I–V in bovine heart mitochondria and the composition of respiratory chain supercomplexes, J. Biol. Chem. 276 (2001) 37861–37867.
[33] S.J. Lee, E. Yamashita, T. Abe, Y. Fukumoto, T. Tsukihara, K. Shinzawa-Itoh, H. Ueda, S. Yoshikawa, Intermonomer interactions in dimer of bovine heart cytochrome *c* oxidase, Acta Crystallogr. Sect. D Biol. Crystallogr. 57 (2001) 941–947.